FimV, ParC and ParP coordinate polar location of the chemosensory arrays in *Pseudomonas putida*

Marta Pulido-Sánchez[a,b†], Aroa López-Sánchez[a,b], Fernando Govantes[a,b#]

Running title: Spatial control of the chemosensory arrays in *Pseudomonas putida*

[a]Centro Andaluz de Biología del Desarrollo, Universidad Pablo de Olavide/Consejo Superior de Investigaciones Científicas/Junta de Andalucía. ES-41013 Sevilla, Spain

[b]Departamento de Biología Molecular e Ingeniería Bioquímica, Universidad Pablo de Olavide. ES-41013 Sevilla, Spain.

[#]Corresponding author

Contact:

Marta Pulido-Sánchez: mpulsan@upo.es

Aroa López-Sánchez: arlopsan@upo.es

Fernando Govantes: fgovrom@upo.es

[†]Current address: Department of Biology, University of Marburg, Marburg, Germany

ABSTRACT

Motile bacteria often rely on chemotaxis systems to promote directional movement in response to specific environmental signals. The chemotaxis machinery is typically arranged in highly ordered polar arrays containing an assortment of chemoreceptors and signal transduction proteins. *Pseudomonas putida* is a polarly flagellated soil bacterium that displays a chemotactic response towards numerous organic compounds present in the rhizosphere. In this work we demonstrate the involvement of the polar landmark proteins FimV, ParC and ParP in the polar assembly of the flagellar motility-associated chemosensory arrays. Confocal microscopy of fluorescent protein fusions and image analysis provide evidence that FimV, ParC, ParP are sequentially recruited to the new cell pole during the cell cycle. This recruitment hierarchy is supported by the observations that FimV is required for ParC localization and FimV and ParC stimulate ParP localization. Bacterial two-hybrid assays suggest the involvement of direct interactions between the three proteins. Our results also show that ParC displays a pole-to-pole oscillatory behavior that results in asymmetric inheritance after cell division. Analysis of the location of the chemoreceptors Aer1 and Aer2 and the histidine kinase CheA illustrates the central role of ParC and ParP in the assembly of polar chemosensory arrays, as both proteins are required for polar recruitment of Aer1 and Aer2 and further promote stable association between CheA and the chemoreceptors at the cell poles.

IMPORTANCE

This work reveals the mechanisms that enable the soil bacterium *Pseudomonas putida* to recruit and assemble the components of its chemotaxis machinery at the new cell pole in the time spanned between two cell divisions. Our findings highlight a complex recruitment hierarchy involving three polar landmark proteins prior the incorporation of the structural components. These observations mirror the assembly sequence of the polar flagella we

recently described in this organism. The correct and timely operation of both mechanisms secures the inheritance of a functional chemotaxis-driven flagellar apparatus by both daughter cells after cell division. There are no previous reports on the mechanisms of polar recruitment and assembly of the chemosensory arrays in the genus *Pseudomonas*.

KEYWORDS

Pseudomonas, chemotaxis, flagellar motility, bacterial cell polarity, ParC, ParP, FimV

INTRODUCTION

Motility is a key evolutionary trait that allows bacteria to explore their surroundings **(Colin *et al*., 2021; Miyata *et al*., 2020)**. Many bacteria are equipped with one or several flagella, semi-rigid helical organelles that emerge from the cell body and rotate to propel them in aqueous or semi-solid media **(Altegoer *et al*., 2014)**. Flagellar rotation enables cells to swim in straight runs interrupted by random reorientation events. In response to chemical gradients bacteria can bias the direction of flagellar rotation to promote efficient navigation towards more favourable environmental conditions. This behavior, known as bacterial chemotaxis, is orchestrated by a conserved set of chemosensors, also known as methyl-accepting chemotaxis proteins (MCPs), and signal transduction proteins assembled in highly organized macromolecular structures known as chemosensory signalling arrays **(Briegel *et al*., 2014; Wadhams and Armitage, 2004; Yang and Briegel, 2020)**.

A typical core chemotaxis unit is composed of a set of transmembrane chemoreceptors organized as trimers of dimers that interact in the cytoplasm with the adaptor protein CheW and the histidine kinase CheA **(Sourjik and Wingreen, 2012)**. Clustering of the core chemotaxis units into hexagonal lattice-like arrays is essential for chemotactic activity, boosting signal sensitivity and integration between different chemosensors **(Wadhams and Armitage, 2004; Sourjik and Wingreen, 2012)**. Similarly structured cytopasmic arrays associated to soluble chemosensors have also been observed **(Thompson *et al*., 2006; Briegel *et al*., 2014)**. Array assembly as first described in *Escherichia coli* is a stochastic process in which individual chemoreceptor proteins randomly insert into the cell membrane and diffuse to eventually join pre-existing clusters or nucleate the formation of new ones **(Greenfield *et al*., 2009; Shiomi *et al*., 2006; Thiem and Sourjik, 2008)**. Many bacterial species localize their chemosensory arrays at the cell poles, although some (e.g., *E. coli*) also bear additional arrays in lateral positions. Location at the cell poles is likely a means to

guarantee segregation to both daughter cells after division **(Jones and Armitage, 2015)**. Multiple mechanisms have been invoked for the polar recruitment and nucleation of the chemosensory components, including stabilization of the structure by the curved membrane or cell pole-specific lipids **(Mileykovskaya and Dowhan, 2000; Thiem *et al*., 2007; Hall *et al*., 2012; Strahl *et al*., 2015)**, or interaction with a variety of polar landmark proteins **(reviewed by Jones and Armitage, 2015)**.

In numerous bacterial species, the positioning and segregation of different macromolecular complexes is mediated by members of the MinD/ParA ATPase family **(reviewed in Pulianmackal and Vecchiarelli, 2024)**. In the polarly flagellated *Vibrio cholerae* and *Vibrio parahaemolyticus*, chemotaxis arrays localize at the flagellated pole, but their distribution shifts to bipolar prior to cell division. Polar localization and cluster formation at the new cell pole is dependent on ParC, a ParA homologue conserved in many γ-proteobacteria, ParP, a CheW domain-containing protein**,** and the polar organizer protein HubP **(Ringgaard *et al*., 2011; Yamaichi *et al*., 2012; Ringgaard *et al*., 2014).** Correct positing of ParC at the cell pole is mediated by HubP, although direct interaction between both proteins was not detected **(Yamaichi *et al*., 2012)**. ParC is found at the flagellated pole in recently divided *V. cholerae* cells and, as cell cycle progresses, forms a second focus at the non-flagellated pole, followed by the chemotaxis proteins CheW1 and CheY3 **(Ringgaard *et al*., 2011)**. ParC is required for proper polar localization of ParP, both proteins have been shown to co-localize and follow the same cell cycle-dependent unipolar/bipolar distribution **(Alvarado *et al*., 2017; Ringgaard *et al*., 2014).**–ParP is in turn required for proper location of diverse components of the chemosensory arrays in *V. parahaemolyticus* and *V. cholerae* **(Ringgaard *et al*., 2014)**. Together, the ParC/ParP system is proposed to anchor the chemotaxis proteins at the cell pole by a diffusion-and-capture mechanism **(Ringgaard *et al*., 2018)**.

Pseudomonas putida is Gram-negative γ-proteobacterium frequently isolated from soils and root-associated microbiomes, used as model organism for bioremediation of organic pollutants due to its extraordinary metabolic versatility **(De Lorenzo *et al*., 2024)**. During its planktonic lifestyle, *P. putida* displays a tuft of 3-6 flagella at a single cell pole that is controlled by the chemotactic response **(Harwood *et al*., 1989)**. Research in the past decades has identified numerous *P. putida* soil isolates that display chemotaxis towards a wide range of aromatic pollutants (**Grimm and Harwood, 1997; Harwood *et al*., 1984, 1990; Lacal *et al*., 2011; Luu *et al*., 2013; Sarand *et al*., 2008)** and other organic compounds present in root exudates **(Canarini *et al*., 2019; López-Farfán *et al*., 2019)**.

P. putida KT2440 possesses 27 different chemoreceptors, and the function of 14 of them has been elucidated so far **(summarized in Rico-Jiménez *et al*., 2022)**. In this strain, most flagellar genes and the core components of the flagella-dependent chemotaxis signal transduction system (**García-Fontana *et al*., 2013; López-Farfán *et al*., 2019)** are encoded in a near-contiguous single genomic region named the flagellar cluster **(Leal-Morales *et al*., 2022)**. A three-tier transcriptional cascade involving the transcription factor FleQ and the alternative σ factor FliA regulates the expression of the flagellar and core chemotaxis signal transduction genes **(Leal-Morales *et al*., 2022)**, and multiple chemoreceptor-encoding genes **(Österberg *et al*., 2010; Rodríguez-Herva *et al*., 2010; Marta Pulido-Sánchez, unpublished).**

Although the intracellular distribution of the core chemotaxis machinery in *P. putida* remains uncharacterized, the Aer1, Aer2 and Aer3 chemoreceptors have been shown to localize at a single cell pole **(Sarand *et al*., 2008)**. Our recent work showed that deletion of the HubP ortholog FimV provokes cells to swim in short, erratic trajectories, reflecting a defect in flagellar function **(Pulido-Sánchez *et al*., 2025)**. We described that FimV is a polar landmark protein present at both *P. putida* cell poles that is recruited to the division site in predivisional cells. FimV is essential to polar localization of the MinD/ParA-type ATPase

FleN, a regulator of the flagella number **(Navarrete *et al*., 2019)**, and they both play a role in synchronizing the assembly of a new set of flagella at the non-flagellated cell pole with the cell cycle. In addition, we showed that FimV stabilizes the polar association of the flagellar landmark protein FlhF, preventing the accumulation of early-flagellar structures at non-polar regions **(Pulido-Sánchez *et al*., 2025)**.

Here, we demonstrate the involvement of FimV, ParC and ParP in the spatial distribution of the chemotaxis arrays in *P. putida* during the cell cycle. Our results indicate that the ParC/ParP system is targeted by FimV to the cell pole, being essential to the chemotactic response by promoting chemoreceptor clustering and stabilizing CheA interaction with the arrays. Our findings shed light on the mechanisms that coordinate the inheritance of the chemosensory arrays associated to the flagellar system in polarly flagellated bacteria.

RESULTS

ParC and ParP are essential for chemotaxis-mediated motility

Homologs of *parC* and *parP* are found within chemotaxis operons in polarly-flagellated γ-proteobacteria **(Ringgaard *et al*., 2011; Ringgaard *et al*., 2014)**The *P. putida* KT2440 flagellar cluster ORFS PP_4334 and PP_4333 **(Leal-Morales *et al*., 2022)** exhibit 51% and 38% identity, and 70% and 56% similarity to *V. cholerae*'s ParC (VC_2061) and ParP (VC_2060), respectively **(Fig. 1A)**. To first identify whether these two proteins contribute to chemotaxis-dependent motility of *P. putida*, we engineered derivatives of KT2442 (a spontaneous rifampicin-resistant mutant of the reference strain KT2440) bearing complete deletions of *parC* and *parP*. The swim diameter of the Δ*parC* and Δ*parP* mutants on soft-agar plates was reduced by 52% and 85% compared to the wild-type strain **(Fig. 1B and C)**. The distribution of flagellar filament tufts in the Δ*parC* and Δ*parP* mutants was indistinguishable from that in the wild-type strain, as observed by confocal microscopy in cells expressing fluorescently labelled FliC **(Fig. S1A and B)**. We next analyzed the chemotactic response of the Δ*parC* and Δ*parP* mutants by performing chemical-in-plug chemotaxis assays **(Parales and Ditty, 2018)** using casamino acids as chemoattractant. Wild-type cells displayed motility halos biased towards the chemoattractant, showing an average chemotactic response index of 1.8 **(Fig. 1D and E)**. However, the Δ*parC* and Δ*parP* mutants exhibited symmetrical halos with response indexes close to 1, indicating that both ParC and ParP are required for the chemotactic behaviour of *P. putida*.

ParC and ParP form a complex with polar landmark FimV at the cell poles

Since ParC and ParP act as polar landmarks for the chemotaxis signalling arrays in *Vibrio* spp. **(Ringgaard *et al.,* 2018)**, we next assessed the intracellular localization of these proteins in *P. putida*. To this end, we constructed miniTn7 derivatives to express ParC and ParP translational fusions to GFPmut3 under the salicylate-inducible P*sal* promoter.

Insertion of the P*sal-parC-gfp* and P*sal-parP-gfp* transposon constructs in the chromosomes of the Δ*parC* and Δ*parP* mutants partially restored the swimming defects of the strains in the absence of salicylate, and salicylate addition improved complementation **(Fig. S2)**. ParC-GFP and ParP-GFP formed polar foci in 84% and 80% of the wild-type cells, respectively, with 60% and 12% of the cells exhibiting foci at both poles, respectively **(Fig. 2A and B)**. Fluorescent foci were never observed at non-polar locations. We analyzed the recruitment of ParC and ParP to the new cell pole during the cell cycle by examining the frequency of cells displaying bipolar distribution of the fluorescently labeled proteins as a function of cell length. Bipolar distribution of ParP-GFP was only observed in cells longer than ~3.5 μm, and its frequency increased steadily with cell length **(Fig. 2C)**, mirroring our previous observations with the late flagellar protein FliC **(Pulido-Sánchez *et al.*, 2025)**. These results suggest that ParP is recruited to the new cell pole during the final steps of flagellar assembly before cell division. In contrast, bipolarly distributed ParC-GFP was prevalent in cells of intermediate size **(Fig. 2C)**. Notably, the absence of ParC polar foci was most prevalent (~50%) in the shorter, postdivisional cells and the frequency diminished with cell growth to ~10% in cells longer than ~3.5 μm **(Fig. 2D)**. This suggests in cells bearing ParC at the old (flagellated) pole the new pole is populated with ParC units at the expense of the old pole, and while this leads to a transient bipolar distribution, eventually the old pole becomes vacant, resulting in ParC association only at the new pole. This inevitably leads to asymmetric segregation, with one daughter cell inheriting ParC nucleated at one pole, and the other one inheriting none.

Next, we examined the impact of ParC on ParP location and vice versa. While deletion of *parP* did not substantially alter the polar distribution of ParC-GFP **(Fig. 2A and B)** or its dynamics in the cell cycle **(Fig. 2C and D)**, Δ*parC* cells displayed a diffuse distribution of ParP-GFP in the cytoplasm, accompanied by localized foci at one or both cell poles in only 29% of the population **(Figs. 2A and B).** Again, ParP-GFP foci were never detected at non-

polar locations. Bipolar ParP-GFP distribution was restricted to a small percentage of very long, predivisional cells in this background **(Fig. 2C)**. These results indicate that ParC is required for efficient recruitment of ParP to the new cell pole.

In *V. cholerae* and *V. parahaemolyticus*, HubP determines the polar localization of ParC **(Yamaichi *et al.*, 2012)**. Lack of the HubP ortholog in *P. putida*, FimV **(Pulido-Sánchez *et al.*, 2025)** provoked a defect in chemotaxis, showing a significant reduction in the chemotactic response index towards the assayed chemoattractant **(Figs. S3A and B)**. Accordingly, we next tested the possible involvement of FimV in the polar localization of ParC and ParP. Thus, we inserted the P*sal-parC-gfp* and P*sal-parP-gfp* transposons in the chromosome of the Δ*fimV* mutant, as well as a P*sal-fimV-gfp* construct into the Δ*parC* and Δ*parP* mutants **(Fig. 2A)**. While the intracellular distribution of FimV-GFP was not altered in the absence of ParC or ParP **(Fig. 2B)**, deletion of *fimV* caused a major disruption in the polar localization of ParC-GFP and ParP-GFP. In the absence of FimV the frequency of cells showing polar ParC-GFP foci dropped to ~5%, with a residual population (<1%) showing foci at both cell poles **(Fig. 2B)**. On the other hand, FimV was not essential for polar localization of ParP-GFP, but the frequency of cells bearing polar foci decreased to 42% in the Δ*fimV* mutant **(Fig. 2B)**. The frequency of Δ*fimV* cells displaying bipolar ParP-GFP foci was also decreased by half **(Fig. 2B)**. In addition to polar foci, we noticed that Δ*fimV* cells displayed diffuse ParP-GFP fluorescence in the cytoplasm **(Fig. 2A)**, reminiscent of the ParP-GFP distribution in the Δ*parC* strain **(Fig. 2A)**.

We next assessed the *in vivo* interactions between the three proteins by way of bacterial adenylate cyclase two-hybrid (BACTH) assays using fusions of the T18 and T25 adenylate cyclase domains to the C-terminal ends of FimV, ParC and ParP, and β-galactosidase activity as reporter **(Fig. 3)**. We observed high β-galactosidase levels in the FimV-FimV and FimV-ParC pairs, and modest β-galactosidase levels the FimV-ParP and ParC-ParP pairs, suggesting that interaction with the polar landmark protein FimV may contribute to polar

recruitment of ParC, while interaction with FimV and ParC may contribute to polar recruitment of ParP. ParC-ParC and ParP-ParP pairs yielded b-galactosidase activity indistinguishable from the negative control, indicating that our assay failed to detect self-interactions of these two proteins.

Because of the shared location of the flagellar and chemotaxis machineries and their related functions, we explored the possibility of cross-talk between ParC and ParP and the regulators of flagellar location and number FlhF and FleN. The intracellular distribution of the fluorescently labeled FlhF-GFP and GFP-FleN **(Pulido-Sánchez *et al*., 2025)** was not altered by the absence of ParC or ParP (**Fig. S4**). Similarly, deletion of *flhF* or *fleN* did not alter the intracellular distribution of ParC-GFP or ParP-GFP (**Fig.S5**), suggesting that both recruitment pathways are independent from each other.

Polar targeting of CheA is mediated by FimV, ParC and ParP

To address how FimV, ParC and ParP contribute to the recruitment of the chemotaxis proteins, we used the histidine kinase CheA as reporter. To assess the intracellular localization of CheA, we engineered a miniTn7 derivative to produce a translational fusion of this protein to GFPmut3 from its natural P*cheA* promoter. Complementarily, we constructed a KT2442 derivative bearing a complete in-frame deletion of the *cheA* gene to assess functional complementation of the fusion protein. The Δ*cheA* mutant did not spread from the inoculation point in soft agar-based swimming in the duration of the standard experiment (12 h) (**Fig. S6A**), but displayed a small motility halo after 48 h incubation **(Fig. S6B)** and single-cell motility tracking revealed that the mutant cells are fully motile, but largely unable to change swimming direction as required for the chemotactic response **(compare Pulido-Sánchez *et al*., 2025, Fig. 2B with Fig. S6C)**. Expression of P*cheA*-*cheA-gfp* restored the ability to display swimming motility halos in the Δ*cheA* mutant (**Fig. S6A**).

By using confocal microscopy, we observed that wild-type cells bearing the P*cheA-cheA-gfp* transposon displayed heterogeneous diffuse fluorescence in the cytoplasm, occasionally accompanied by polar foci (**Fig. S7**). In contrast, polar CheA-GFP foci were clearly evident in most cells the Δ*cheA* mutant, with little residual fluorescence in the cytoplasm **(Fig. 4A)**. We attribute these differences to an apparent competitive advantage of the native CheA protein in its association to the cell poles. Consequently, we further performed CheA-GFP microscopy imaging in Δ*cheA* strains. The vast majority (~99%) of Δ*cheA* cells exhibited polar CheA-GFP foci **(Fig. 4A and B)** and ~20% displayed a bipolar distribution. Deletion of *parC*, *parP* or *fimV* in this background only caused a small decrease (5-12%) in the frequency of polar foci, and only the Δ*fimV* mutant displayed somewhat higher (~30%) frequency of the bipolar distribution, indicating that none of these proteins are strictly required for the recruitment of CheA to the cell poles **(Fig. 4A and B)**. The frequency of cells displaying ectopic CheA-GFP foci increased by 60% in the absence of *parC* and by 34% in the absence of *fimV* **(Fig. 4C)**, accompanied by a general decrease in the fluorescence intensity of the polar foci **(Fig. 4D)**. On the other hand, deletion of *parP* resulted in a more diffuse distribution of CheA-GFP in the cell cytoplasm **(Fig. 4A)** and less accumulation of the fluorescent protein at the cell poles **(Fig. 4D)**. When examining the frequency of bipolar CheA-GFP distribution relative to cell length in the Δ*cheA* mutants, we observed that the frequency increased steadily with cell length to a maximum ~80% in long, predivisional cells **(Fig. 4E)**, suggesting that CheA is recruited to the new cell pole while it remains permanently associated to the old cell pole, as previously observed with flagellar proteins **(Pulido-Sánchez *et al*., 2025)**. This pattern is unaltered in the absence of FimV. However, deletion of *parC* or *parP* resulted in CheA-GFP accumulation stalling at 40-50% bipolar distribution in cells longer than ~4 µm **(Fig. 4E).** In addition, CheA accumulation was more prevalent in shorter cells in the absence of ParC. These results suggest that CheA can spontaneously locate at the cell poles, but this association is temporary and in a dynamic equilibrium with

the cytoplasmic CheA pool. At the early stages of the cycle ParC limits CheA interaction with the cell pole, but polar recruitment of ParP at the later stages boosts permanent association of CheA with the cell poles likely by promoting its assembly into the chemotaxis arrays. We also assessed the impact of CheA on the location of ParC-GFP and ParP-GFP **(Fig. S8)**, but no changes in the intracellular distribution of both proteins were evident, suggesting that CheA does not contribute to the polar location of ParC or ParP.

ParC, ParP and CheA are required for polar clustering of the chemoreceptors

To evaluate the role of the ParC/ParP system in the localization of the chemotaxis chemoreceptors in *P. putida*, we engineered translational fusions to *yfp* at the 3' end of the *aer1* and *aer2* chemoreceptor-encoding genes at their genomic *loci* in the wild-type strain and the Δ*parC*, Δ*parP* and Δ*fimV* mutants, as previously described **(Sarand *et al*., 2008)**. Confocal microscopy revealed that in wild-type cells, Aer1-YFP and Aer2-YFP were diffusely distributed along the cell contour (**Figs. 5A and B and S9**), but particularly accumulated as foci at the cell poles in 90-95% of the cells, with 1-2% displaying foci at both poles **(Fig. 5C)**. Bipolar distribution of Aer1-YFP and Aer2-YFP was only observed in cells longer than ~3.5 µm, and their frequency increased steadily with cell length **(Fig. S10)**, as shown above with ParP **(Fig. 2C)** and previously with the flagellin FliC **(Pulido-Sánchez *et al*., 2025)**. In contrast, polar accumulation of both proteins was absent in the Δ*parC* and Δ*parP* strains **(Fig. 5A, B and C)**, indicating that the formation of polar chemosensory arrays is strictly dependent on the ParC/ParP system. We did not observe major changes in the distribution of both MCPs at the cell contour in the Δ*fimV* mutant, as only a small increase in the frequency of bipolar Aer2-YFP foci was observed in this background **(Figs. 5A, B and C)**. Deletion of FimV however caused a decrease in the intensity of the Aer1-YFP and Aer2-YFP foci, suggesting that it may directly or indirectly stimulate the recruitment or stabilize the association of the chemoreceptors to the cell poles.

Similarly, we examined whether CheA plays a role in the polar location of both chemoreceptors. Aer1-YFP and Aer2-YFP were still able to locate at the cell contour and form polar foci in the absence of *cheA* **(Fig. 5A and B)**. Fluorescence at the cell contour was modestly increased in comparison to the wild-type strain **(Fig. 5B)**, and the frequency of cells bearing polar foci was somewhat diminished **(Fig. 5C and S10)**. In addition, we observed a reduction in the fluorescence intensity of the polar foci for both proteins in the mutant background **(Fig. 5D),** suggesting that CheA is not strictly required for polar location, but promotes polar clustering of the chemoreceptors at the chemosensory arrays.

DISCUSSION

Despite their lack of internal compartments, prokaryotic cells are highly organized, with related functional elements often recruited to specific cellular locations to achieve maximum efficiency **(Surovtsev and Jacobs-Wagner, 2018; Rudner and Losick, 2010)**. The delivery of the components of the bacterial chemosensory systems to particular regions in the cell envelope and their assembly into intricate arrays containing multiple sensory elements along with the signal transduction system required to translate the signals detected into a coherent behavior is but one example of such elaborate intracellular organization **(reviewed by Jones and Armitage, 2015)**. Here we present evidence of the involvement of the polar landmark proteins FimV, ParC and ParP to the stable recruitment of the components of the chemosensory apparatus to the cell poles of *P. putida* to form functional chemosensory arrays in the vicinity of the polar flagellar apparatus during its assembly. By coordinately assembling the flagella and associated chemosensory machinery in the timespan of one cell cycle, polarly flagellated bacteria ensure the inheritance of fully functional motility and chemotaxis systems by both daughter cells after cell division.

Our results demonstrate that the polar clustering required for full functionality of the chemosensory arrays is driven by the interaction between three polar landmark proteins: FimV, ParC and ParP. We recently showed that FimV is required for the polar location of the flagellar number regulator FleN and contributes to the stability of the association of the flagellar landmark protein FlhF with the cell poles **(Pulido-Sánchez *et al.*, 2025)**. Here we show that (i) deletions of *parC* or *parP* strongly impair swimming motility and fully abolish positive chemotaxis in agar plate-based assay, while *fimV* deletion decreases such chemotactic response **(Figs. 1 and S3)** (ii) FimV is essential to polar recruitment of ParC and both FimV and ParC contribute to the polar location of ParP **(Fig. 2)**; and (iii) all three proteins display evidence of mutual interaction (albeit with varying intensity) in the bacterial two-hybrid BACTH assay **(Fig. 3)**. Our results suggest that FimV is the polar landmark

protein at the top of the recruitment hierarchy. FimV is present at the cell equator during cell division and then remains permanently associated to the emerging cell poles **(Pulido-Sánchez *et al*., 2025)**. FimV is required to recruits ParC to the new cell pole during early cell growth, as evidenced further by the sharp FimV-dependent increase in the frequency of bipolar ParC-GFP distribution in this period **(Fig. 2C)**, likely by direct protein-protein interaction **(Fig. 3)**. Next, FimV and ParC boost the asociation of ParP with the cell pole by either increasing the natural ability of ParP to bind at this location or stabilizing its association with the cell pole. The mechanisms involving HubP (an ortholog of FimV), ParC and ParP in the polar localization and proper inheritance of the chemotaxis arrays in polarly flagellated bacteria have been explored in *V. cholerae* and *V. parahaemolyticus* **(Ringgaard *et al*., 2011; Yamaichi *et al*., 2012; Ringgaard *et al*., 2014; Alvarado *et al*., 2017; Mauriello *et al*., 2018)** and *Shewanella putrefaciens* **(Rossmann *et al*., 2015)**. These works also demonstrated the presence of a three-tiered HubP>ParC>ParP hierarchy. However, the interactions that we observe between FimV, ParC and ParP in *P. putida* differ from those reported in the *Vibrio* spp. Firstly, interaction between HubP and ParC was not detected in these organisms, and an additional protein was proposed to act as a linker **(Ringgaard *et al*., 2018; Yamaichi *et al*., 2012)**. Secondly, unlike their orthologs in *Vibrio* spp. **(Ringgaard *et al*., 2014; Yamaichi *et al*., 2012)**, ParC and ParP do not cluster at non-polar locations in the *P. putida* Δ*fimV*, Δ*parC* or Δ*parP* mutants, but always appear at the cell poles and/or dispersed in the cytoplasm. Finally, we have shown that ParC localization is independent on ParP, while ParP enhances polar anchoring of ParC in *Vibrio* spp. **(Ringgaard *et al*., 2014)**.

Our results show that ParC and ParP localize at the cell poles in ~80% of the wild-type population **(Fig. 2B)**, but quantitative image analysis indicates that they follow different distribution dynamics during the cell cycle. The predominant unipolar distribution of ParP is only shifted to bipolar in longer, predivisional cells cells (>3.8 μm) **(Fig. 2C)**, following a trend reminiscent of the bipolar distribution of the flagellar filament protein FliC **(Pulido-Sánchez**

***et al*., 2025)**. In contrast, the ParC bipolar distribution emerges at the beginning of the cell cycle to reach a maximum frequency in cells of intermediate length, and drop again in longer, predivisional cells **(Fig. 2C)**. In addition, ~50% of the shorter, postdivisional cells lacked polar ParC-GFP foci **(Fig. 2D)**, suggesting that ParC is located at a single pole at the time of cell division and only one of the daughter cells can inherit the polarly located protein. In *V. cholerae*, ParC is recruited to the new cell pole after cell division as a result of redistribution of ParC molecules bound to the old pole by way of a diffusion-and-capture mechanism to achieve a bipolar distribution at the equilibrium in the longer, predivisional cells **(Ringgaard *et al*., 2011)**. The characteristic pattern observed in *P. putida* suggests that a modified version of the above mechanism operates in this organism. We propose that diffusion from the old pole to the cytoplasm and recapture at the new pole is also responsable for ParC recruitment to the new pole. However, recapture at the old pole is inhibited, and therefore ParC progressively accumulates at the new pole as it becomes depleted from the old pole, resulting in a transient bipolar distribution that evolves into a unipolar distribution with ParC located only at the new pole at the end of the cycle **(Fig. 6A)**. This mechanism is reminiscent of the pole-to-pole oscillatory behavior of the positional cell division regulatory proteins MinC and MinD **(Hu and Lutkenhaus, 2002; Raskin and de Boer, 1999; Rowlett and Margolin, 2013)**. Eviction of ParC from the old pole strongly suggest that its polar location is likely unnecessary for chemotaxis array function beyond the assembly stage. As a consequence of this mechanism, the newly-divided daughter cell that lacks pole-bound ParC would require *de novo* ParC polar targeting at early stages of the cell cycle. A similar behavior was previously observed with the *P. aeruginosa* diguanylate cyclase HsbD **(Valentini *et al*., 2016)**.

We have also examined the contribution of FimV, ParC and ParP to the polar location of the chemotaxis machinery components. The kinase/phosphotransferase protein CheA is part of the signal transduction pathway of chemotaxis and a cytoplasmic component of the

chemosensory arrays **(Muok *et al*., 2020; Wadhams and Armitage, 2004)**. Aer1 and Aer2 are two chemoreceptors similar to *E. coli* Aer **(Sarand *et al*., 2008)**. Our results show that CheA, Aer1 and Aer2 accumulate at polar locations in the vast majority of wild-type cells **(Fig. 4A and B and 5A and C)**. While the overall ability of CheA to associate to the cell poles is not greatly affected by the presence of FimV, ParC or ParP **(Fig. 4A and B)**, full extent CheA accumulation is not attained in their absence **(Fig. 4D)**, suggesting that CheA can spontaneously associate the cell poles, but the polar landmark proteins are required for stabilization of the interaction. In contrast, polar nucleation of Aer1 and Aer2 is strictly dependent on the presence of ParC and ParP **(Fig. 5, A-C)**, while FimV and CheA contribute to stabilize the association between the chemoreceptors and the cell pole **(Fig. 5D and Fig. S10)**. The intracellular distribution of ParP, CheA, Aer1 and Aer2 shifted from unipolar to bipolar with increasing cell length **(Figs. 4E and S10)**, suggesting permanent association to the old (flagellated) pole and progressive occupancy of the new (non-flagellated) pole **(Pulido-Sánchez *et al*., 2025)**. ParP-GFP only displayed a bipolar distribution in cells longer than 4 µm **(Fig. 2C)**. A similar distribution was observed with Aer1-YFP and Aer2-YFP in wild-type cells, but was abolished in the absence of ParP **(Fig. S10)**. Polar localization of CheA was inhibited by ParC in shorter cells, but was stabilized by ParC-dependent recruitment of ParP at later stages **(Fig. 4E)**. We propose that the interplay between ParC and ParP promotes timely, permanent association of CheA with the new pole specifically in long, predivisional cells. The temporal and spatial coincidence of ParP, CheA and the MCPs at the cell poles and their dependence relationships for recruitment and stabilization are fully consistent with the model proposed for *V. cholerae* and *V. parahaemolyticus*. In these organisms, ParP interacts directly with CheA and the chemoreceptors to stabilize the polar association of CheA, prevent diffusion of the chemoreceptors in the cell membrane and promote their assembly into the chemosensory arrays at the cell poles **(Ringgaard *et al.*, 2014; Alvarado *et al*., 2017; Ringgaard *et al*., 2018)**.

Taken together, our evidence supports the notion that the ParC/ParP system is accountable for the formation of the chemosensory arrays at the cell poles in *P. putida*, as previously reported in *Vibrio* spp. **(Ringgaard *et al.*, 2014; Alvarado *et al.*, 2017; Ringgaard *et al.*, 2018)**. Nevertheless, some of the interactions between the proteins mediating this process deviate from those described in *Vibrio*, as discussed above. We propose that FimV captures cytoplasmic ParC at the new cell pole where flagella assembly is taking place during the early stages of the cell cycle **(Fig. 6B)**, while CheA associates and dissociates spontaneously from the cell pole. This association dynamics may be supported by transient interactions with MCPs diffusing at the cell membrane and is limited by the presence of ParC. At a later stage, ParC facilitates polar targeting of ParP concomitantly and in turn, ParP directs polar assembly of the chemosensory signalling arrays by recruiting the chemosensory components. The stabilizing effects of ParP and CheA on the polar association of CheA and the chemoreceptors, respectively, reflects the driving role of ParP in the assembly of the chemosensory array, as described in *V. parahaemolyticus* and *V. cholerae* **(Ringgaard *et al.*, 2014; Alvarado *et al.*, 2017; Ringgaard *et al.*, 2018)**. In summary, our results strongly support a model in which the assembly of the chemotaxis arrays arises from the collaborative interactions between FimV, ParC and ParP with the chemoreceptors and the chemotaxis signal transduction proteins.

Positioning of the chemosensory arrays at or near the cell poles has been vindicated as a safe means to guarantee inheritance of chemotaxis functionality by both offspring upon cell division **(Jones and Armitage, 2015)**. The elegant mechanisms previously described for *Vibrio* spp. **(Ringgaard *et al.*, 2011; Yamaichi *et al.*, 2012; Ringgaard *et al.*, 2014; Alvarado *et al.*, 2017)** and herein for *P. putida* attain this goal by coupling the *de novo* assembly of chemotaxis arrays at the new cell pole to the progress of the cell cycle. Because both *Vibrio* and *Pseudomonas* spp. bear polar flagella, the chemosensory arrays are located in close vicinity to the flagellar apparatus. The findings reported here mirror our previous

work with the *P. putida* polar flagella **(Pulido-Sánchez *et al*., 2025)**. Flagella are also sequentially assembled at the new pole in the duration of a cell cycle in preparation for cell division. Both processes are initiated by FimV and involve the recruitment of a MinD/ParA family protein (ParC and FleN, respectively), and an additional protein (ParP and FlhF) responsible for the initial recruitment of the structural components. The correct and timely operation of these mechanisms secures the inheritance of a functional chemotaxis-driven flagellar apparatus by both daughter cells after cell division.

MATERIALS AND METHODS

Bacterial strains and growth conditions

Bacterial strains used in this work are listed in **Table S1.** Liquid cultures of *Escherichia coli* and *P. putida* were routinely grown in lysogeny broth (LB) **(Sambrook and Russel, 2000)** with 180 rpm shaking at 37 ºC and 30 ºC, respectively. Minimal medium was prepared as previously described **(Mandelbaum *et al*., 1993)** containing lactose (25 mM) and ammonium chloride (1000 mg l^{-1}) as the sole carbon and nitrogen sources. For solid media, 1.5% American Bacteriological Agar (Condalab) was added prior to autoclaving. When appropriate, antibiotics and other compounds were added at the following concentrations: ampicillin (100 mg l^{-1}), carbenicillin (500 mg l^{-1}), chloramphenicol (15 mg l^{-1}), gentamycin (10 mg l^{-1}), rifampicin (20 mg l^{-1}), kanamycin (25 mg l^{-1}, or 50 mg l^{-1} when using *E. coli* BTH101 as host strain), 3-methylbenzoate (3MB) (3 mM), 5-bromo-4-chloro-3-indoyl-β-D-galactopyranoside (X-gal) (25 mg l^{-1}), isopropyl β-D-1-thiogalactopyranoside (IPTG) (1 mM), sodium salicylate (2 mM). All reagents were purchased from Sigma-Aldrich.

Plasmid and strain construction

Plasmids and oligonucleotides used in this work are listed in **Table S1**. DNA manipulations were conducted following standard protocols **(Sambrook and Russell, 2000)**. Restriction and modification enzymes were used following the manufacturer's instructions (New England Biolabs). PCR amplifications were performed using Q5® High-Fidelity DNA Polymerase (New England Biolabs) for cloning purposes, and DreamTaq™ DNA Polymerase (Thermo Fischer) to check plasmid constructions and chromosomal manipulations. *E. coli* DH5α was used as host strain for cloning procedures. Cloning steps involving PCR were verified by commercial Sanger sequencing (Stab Vida). Plasmid DNA was transferred to *E. coli* strains by transformation **(Inoue *et al*., 1990)** or electroporation **(Dower *et al*., 1988)**, and to *P. putida* by triparental mating **(Espinosa-Urgel *et al.,* 2000)**

or electroporation **(Choi *et al.,* 2006)**. Site-specific integration of miniTn7-derivatives at the single *att*Tn7 chromosomal site in *P. putida* strains was performed and PCR-verified as previously described **(Choi *et al.,* 2005)**. Specific details of plasmid and strain construction are provided as **Supplementary Materials and Methods**.

Swimming motility assays

Swimming assays were adapted from Parkinson **(Parkinson, 1976)** Fresh colonies were toothpick-inoculated in Tryptone-agar plates (1% Bacto™ Tryptone [Difco], 0.5% NaCl, 0.3% Bacto™ Agar), and incubated at 30 ºC for 12 h or 48 h. Medium was supplemented with sodium salicylate when required. Digital images were taken and swimming halos diameter were measured using GIMP v2.10.10 **(The GIMP Development Team, 2019)** and normalized to the wild-type.

Chemotaxis assays

Quantitative chemical-in-plug chemotaxis assays were performed as previously described **(Parales and Ditty, 2018)** with some modifications. Plugs of 2% agarose prepared in chemotaxis buffer (25 mM Na_2HPO_4, 25 mM KH2PO4, 0.05% glycerol, 10 µM EDTA, pH 7.0) containing 0.2% casamino acids as chemoattractant were placed onto the center of 60x15 mm Petri dishes. Plates were poured with 10 mL of chemotaxis buffer containing 0.2% noble agar and allowed to solidify at room temperature for 1 h. Overnight cultures were 250-fold diluted in LB medium and grown to exponential phase (OD_{600} of 0.4-0.5). Cells were harvested by centrifugation (3500 *g*, 10 min, room temperature), washed three times with 1 mL of chemotaxis buffer by gently pipetting to minimize flagella breakage, and adjusted to an OD_{600} of 20. Plates were inoculated by pipetting 2 µL of cell suspensions into the soft agar medium and incubated at 30 ºC for 12 h. Digital images and halo measurements were taken as described above. Chemotaxis response indexes were calculated as the distance from the inoculation point to the edge of the motility halo closest

to the agarose plug, divided by the distance from the inoculation point to the edge of the halo farthest from the agarose plug.

Bacterial Adenylate Cyclase Two-Hybrid (BACTH) assays

Protein-protein interactions were analyzed using a bacterial two-hybrid approach as previously described **(Karimova *et al.*, 1998).** Briefly, the proteins to be tested were fused to the T18 and T25 fragments of the adenylate cyclase catalytic domain of *Bordetella pertussis*. Electrocompetent *E. coli* BTH101 cells were prepared as described **(Karimova *et al.*, 1998; 2000)** and transformed with the corresponding pUT18 and pKNT25/pKT25-derived plasmids by electroporation. Plates were incubated at 30 ºC for 48 h. Three independent colonies were inoculated into the wells of a 96-well polystyrene plate containing 150 µL LB supplemented with ampicillin, kanamycin and IPTG, and subsequently incubated at 30 ºC with 180 rpm shaking for 24 h. Drops containing 10 µL of cell cultures were placed on minimal medium-based agar plates supplemented with X-gal. Plates were incubated at 30 ºC for 4 days and colonies were documented by digital imaging. To quantify the adenylate cyclase activity reconstructed by the interacting hybrid proteins, 100 µL of cell samples withdrawn from the 96-well plates were permeabilized with sodium dodecyl sulfate and chloroform, and β-galactosidase activity was determined as described **(Miller, 1993)**.

Tracking of swimming trajectories

Continuous videos of near-surface cell motility were recorded using a Leica DMI4000B inverted microscope equipped with a Leica HCX PL FLUOTAR 20x/0.40 CORR PH1 objective lens and a Leica DFC360 FX CCD camera (pixel size: 0.2012 µm). Overnight LB cultures were 250-fold diluted in the same medium and grown to an OD_{600} of 0.3. Serial dilutions 10^3 to 10^5 were prepared and 150 µL samples were transferred to the wells of a Costar® 96-well polystyrene plate (Corning). Brightfield videos of cells swimming on the plane of the well surface were recorded for 1 min, and converted to 4 fps time-lapses using

ImageJ (Fiji) v1.53t **(Schneider *et al*., 2012)**. Trajectories of 20 cells of each strain were tracked for 15 s using the Manual Tracking v2.1.1 plugin.

Confocal microscopy and image analysis

Overnight cultures were 100-fold diluted in LB medium supplemented with 2 mM salicylate when necessary and grown to an OD_{600} of ~0.5. Cells from 1 mL samples were harvested by centrifugation (5000 *g*, 5 min, room temperature) and washed three times with 1 mL PBS. Flagellar filaments of strains expressing $FliC^{S267C}$ were stained by carefully resuspending cells in PBS supplemented with 5 µg/mL Alexa Fluor™ 488 C5 Maleimide (Molecular Probes) **(Hintsche *et al*., 2017)**. After 5 min incubation in the dark, cells were washed three times for excess dye removal. For membrane staining, cells were resuspended in 100 µL of PBS containing 5 µg/mL FM™ 4-64 (Molecular Probes) and incubated for 5 min in the dark. Drops of 2 µL samples were immediately placed on 1% agarose pads prepared with deionized water to be imaged using an Axio Observer7 confocal microscope (Zeiss) equipped with a CSU-W1 spinning disk module (Yokogawa). Images were taken using a Zeiss α Plan-Apochromat 100x/1.46 Oil DIC M27 objective lens and a Prime 95B CMOS camera (Teledyne Photometrics, pixel size: 0.1099 µm), controlled by the SlideBook 6 software. GFPmut3 and Alexa Fluor™ 488 fluorescence were excited with the 488 nm laser line and collected with emission filter 525/50 nm, setting exposure times at 300 and 100 ms, respectively. YFP fluorescence was excited at 514 nm and collected with a 525/50 nm filter (300 ms exposure time). FM™ 4-64 was excited at 561 nm and fluorescence was collected with a 617/73 filter (1000 ms exposure time). For each image, seven Z-sections were taken with a step size of 0.33 µm.

Microscopy images were processed using ImageJ (Fiji) v1.53t **(Schneider *et al*., 2012)** and analyzed using the MicrobeJ v5.13I plugin **(Ducret *et al*., 2016)** following a previously described pipeline **(Pulido-Sánchez *et al*., 2025)**. Additionally, cell contour axis profiles were recorded with MicrobeJ using default parameters and setting a dilate value of 0.2 µm.

Bioinformatics analyses

Sequence alignments were carried out using the MUSCLE tool from the EMBL-EBI website (https://www.ebi.ac.uk/jdispatcher/msa/muscle) **(Madeira *et al*., 2024)**. Similarity between *P. putida* KT2440 and *V. cholerae* O1 El Tor ParC and ParP proteins was scored using the BLASTp tool from the NCBI website (blast.ncbi.nlm.nih.gov/Blast.cgi) **(Altschul *et al*., 1990).**

Statistical analysis

Statistical data treatment was performed using GraphPad Prism v8.3.0 software. Results are reported as the average and standard deviation of at least three biological replicates, or as the median and 95% confidence interval for the median in foci fluorescence quantification. Significance (p-values) of the differences among strains/samples was evaluated by means of the two-tailed Student's t-test for unpaired samples not assuming equal variance.

ACKNOWLEDGMENTS

We wish to thank Antonio Leal-Morales for his help in some of the constructions used in this work, Victoria Shingler for providing the pVI1811 and pVI812 plasmids, Katherina García from the Microscopy Facility at CABD (Sevilla, Spain) for excellent technical assistance, and Kai Thormann for thoughtful advice and discussion. This work was supported by grants PGC2018–097151-B-I00, PID2021–126121-NB-I00 and CEX2020–00108-M from the Spanish Ministerio de Ciencia, Innovación y Universidades/Agencia Española de Investigación (MCIN/AEI) and the European Regional Development Fund “A way of making Europe” (ERDF), and by a predoctoral Formación de Profesorado Universitario contract 19/02899 of the Spanish Ministerio de Educación y Formación Profesional, awarded to M P-S.

FIGURES

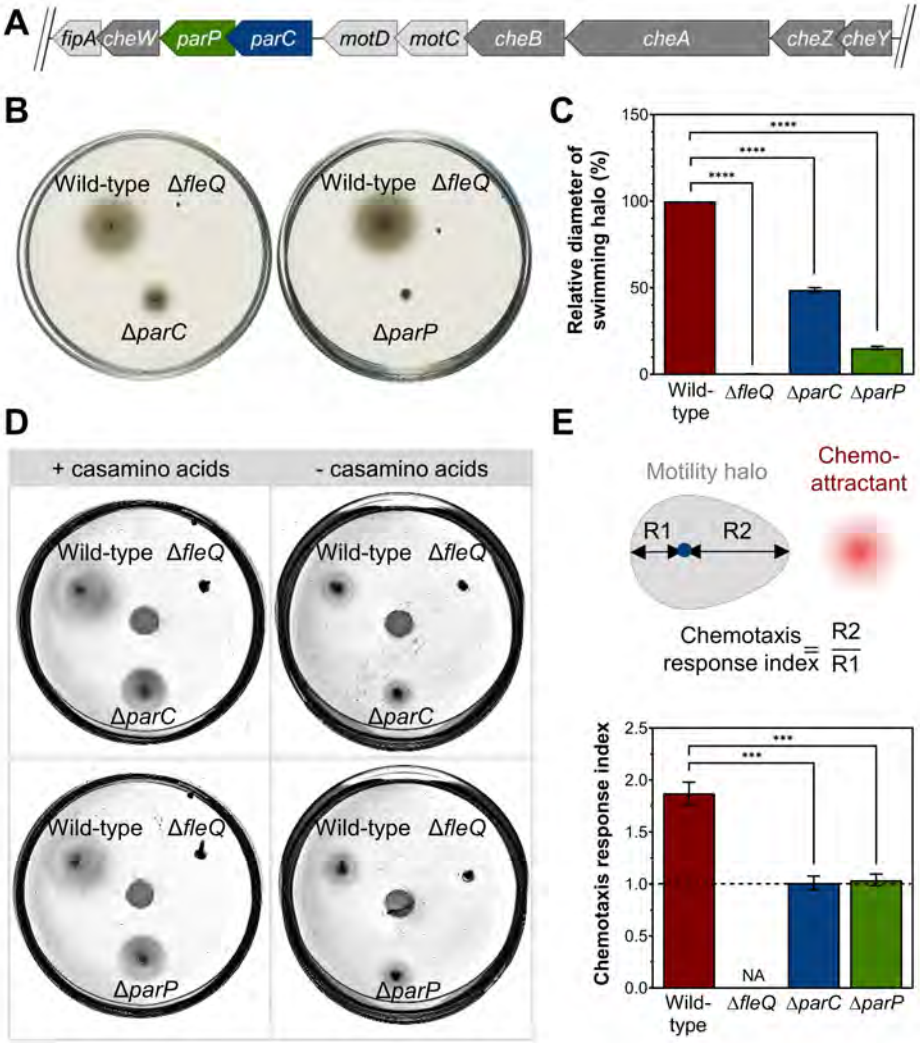

Figure 1. Swimming motility and chemotaxis assays of the Δ*parC* and Δ*parP* mutants. A. Scheme showing the genomic context of the *parC* and *parP* genes in the *P. putida* KT2440 chromosome. Dark grey: chemotaxis machinery-encoding genes. Light grey: flagellar apparatus-related genes. **B.** Soft agar-based swimming motility assays of the Δ*parC* and Δ*parP* mutants. **C.** Motility halo diameters. **D.** Chemical-in-plug chemotaxis assays of the aforementioned strains placing an agarose plug with (left) or without (right) 0.2% casamino acids in the centre of the plate. **E.** Cartoon depicting the calculation of the chemotaxis response index (top) and chemotaxis response indexes of the wild-type strain, and the Δ*parC* and Δ*parP* mutants when exposed to an agarose plug containing casamino acids (bottom). The wild-type strain and the Δ*fleQ* mutant were assayed in the same plates as positive and negative controls. Each picture shows a representative swim plate out of at least three biological replicates. Columns and error bars represent the averages and standard deviations of at least three biological replicates. NA: not applicable. Stars designate p-values for the Student's t-test for unpaired samples not assuming equal variance (*:$p<0.05$; **:$p<0.01$; ***:$p<0.001$; ****:$p<0.0001$).

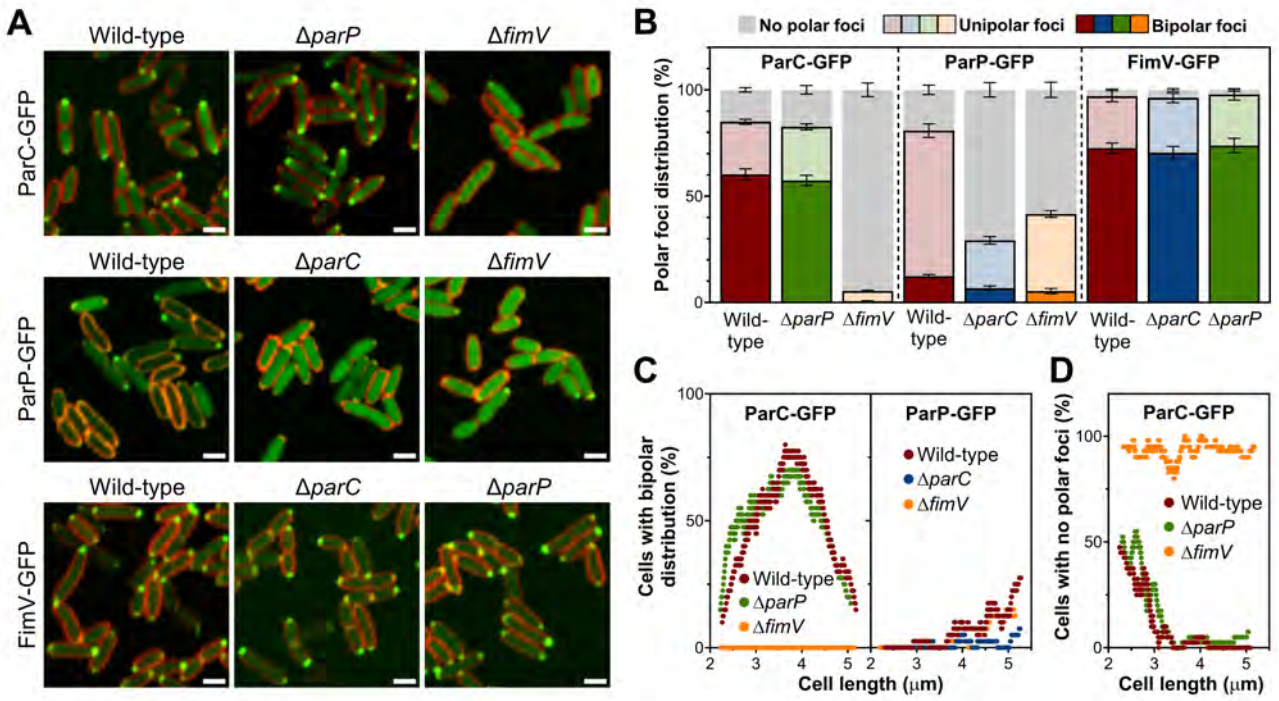

Figure 2. Intracellular location of ParC, ParP and FimV. A. Confocal microscopy images of wild-type, Δ*parC,* Δ*parP* and Δ*fimV*.cells expressing P*sal-parC-gfp*, P*sal-parP-gfp* or P*sal-fimV-gfp* (green) in the absence (FimV) or the presence (ParC and ParP) of 2 mM salicylate. FM^{TM} 4-64 was used as membrane stain (red). Images are shown as the maxima projections of seven Z-sections of the green channel, merged with the red channel showing the cell contour at the focal plane. Scale bar: 2 μm. **B.** Frequency of cells of the aforementioned strains bearing bipolar, unipolar o no polar ParC-GFP, ParP-GFP or FimV-GFP foci. **C.** Frequency of cells of the aforementioned strains displaying bipolar distribution of ParC-GFP or ParP-GFP foci *vs.* cell length. Columns and error bars represent the averages and standard deviations of at least three separate replicates. **D.** Frequency of cells of the aforementioned strains displaying no polar ParC-GFP foci *vs.* cell length (n = 500 cells).

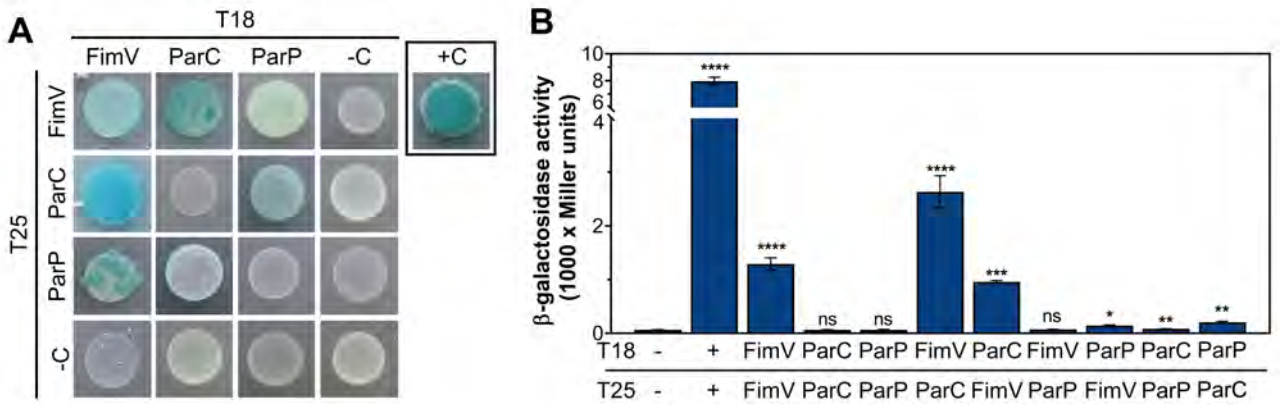

Figure 3. Bacterial two-hybrid assays between FimV, ParC and ParP. A. Interaction drop-assays between FimV, ParC and ParP proteins fused to adenylate cyclase fragments T18 and T25 in the the *E. coli* BTH101 reporter strain. Colonies were grown in minimal medium supplemented with lactose and X-gal. Colony growth and blue colour denote positive interaction between each pair of hybrid proteins. Co-transformants expressing pUT18 and pKNT25 empty vectors, or pUT18-zip and pKNT25-zip were used as negative and positive controls, respectively. Each picture shows a representative colony out of at least nine biological replicates. **B.** Quantification of the interaction strength by β-galactosidase assays. Columns and error bars represent the averages and standard deviations of at least three biological replicates. Stars designate p-values for the Student's t-test for unpaired samples not assuming equal variance (ns: non-significant; *:$p<0.05$; **:$p<0.01$; ***:$p<0.001$; ****:$p<0.0001$).

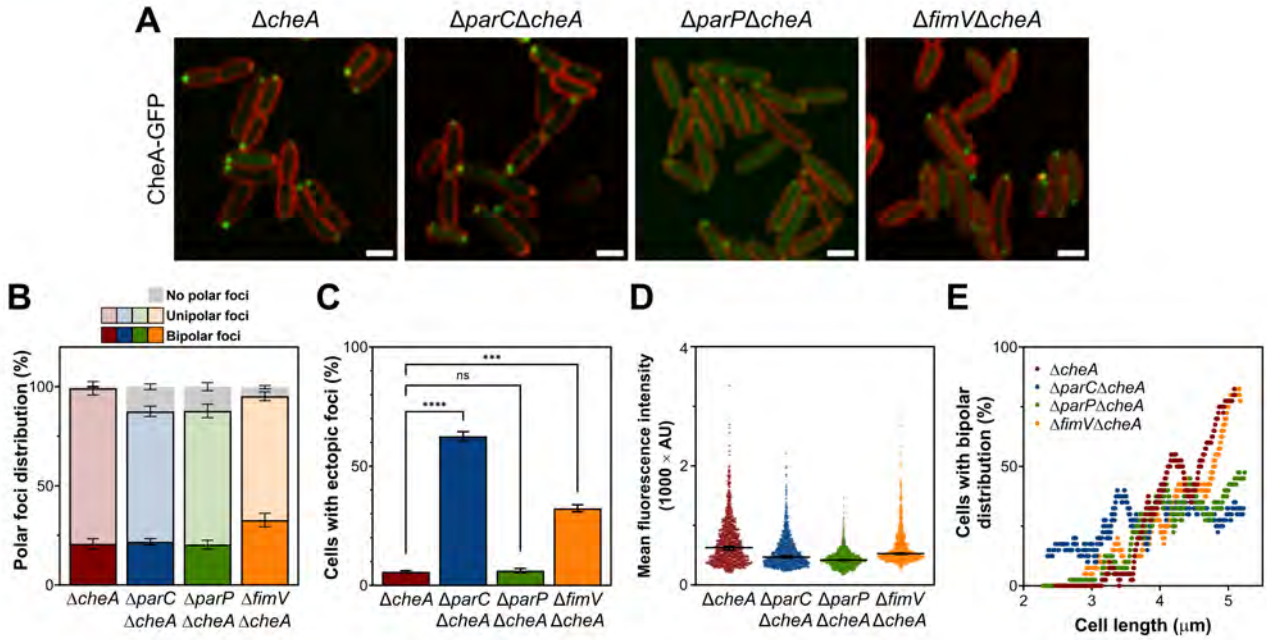

Figure 4. Intracellular location of CheA. A. Confocal microscopy images of Δ*cheA*, Δ*parC*Δ*cheA*, Δ*parP*Δ*cheA* and Δ*fimV*Δ*cheA* cells expressing P*cheA-cheA-gfp* (green). FM™ 4-64 was used as membrane stain (red). Images are shown as the maxima projections of seven Z-sections of the green channel, merged with the red channel showing the cell contour at the focal plane. Scale bar: 2 μm. **B.** Frequency of cells of the aforementioned strains bearing bipolar, unipolar o no polar CheA-GFP foci. **C.** Frequency of cells of the aforementioned strains bearing non polar CheA-GFP foci. **D.** Mean fluorescence intensity of polar CheA-GFP foci in the aforementioned strains. **E.** Frequency of cells of the aforementioned strains displaying bipolar distribution of CheA-GFP foci *vs.* cell length. Columns and error bars represent the averages and standard deviations of at least three separate replicates. Points correspond to individual fluorescence intensity values, bars denote the median and the 95% confidence interval for the median (n = 500 cells). Stars designate p-values for the Student's t-test for unpaired samples not assuming equal variance (ns: non-significant; *:p<0.05; **:p<0.01; ***:p<0.001; ****:p<0.0001).

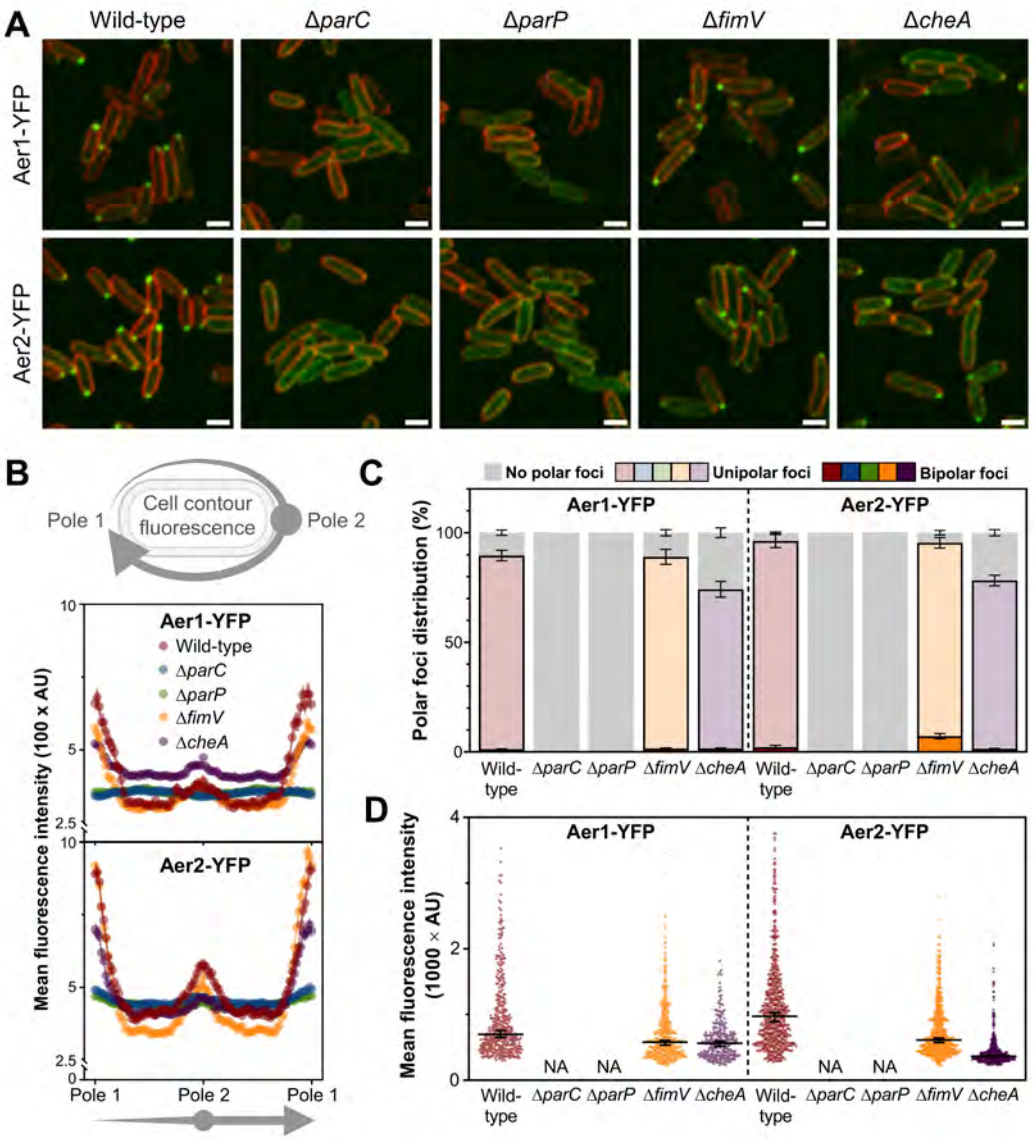

Figure 5. Intracellular location of MCPs. A. Confocal microscopy images of wild-type, Δ*parC*, Δ*parP*, Δ*fimV* and Δ*cheA* cells expressing *aer1-yfp* or *aer2-yfp in locus* (green). FM^{TM} 4-64 was used as membrane stain (red). Images are shown as the maxima projections of seven Z-sections of the yellow channel, merged with the red channel showing the cell contour at the focal plane. Scale bar: 2 µm. **B.** Distribution of Aer1-YFP and Aer2-YFP fluorescence along the cell contour of cells of the aforementioned strains. The x-axis displays the relative position along the cell contour following the path depicted by the upper scheme: the axis origin represents the cell pole with the highest fluorescence intensity (pole 1), mid-axis represents the pole with the lowest fluorescence intensity (pole 2), and right-end represents again pole 1. **C.** Frequency of cells of the aforementioned strains bearing bipolar, unipolar o no polar Aer1-YFP and Aer2-YFP foci. **D.** Mean fluorescence intensity of polar Aer1-YFP and Aer2-YFP foci in the aforementioned strains. Points and shaded areas in panel **B** represent average and standard error of the mean of at least three separate replicates. Points in panel **D** correspond to individual fluorescence intensity values, bars denote the median and the 95% confidence interval for the median. Columns and error bars represent the averages and standard deviations of at least three separate replicates (n = 500 cells). NA: not applicable.

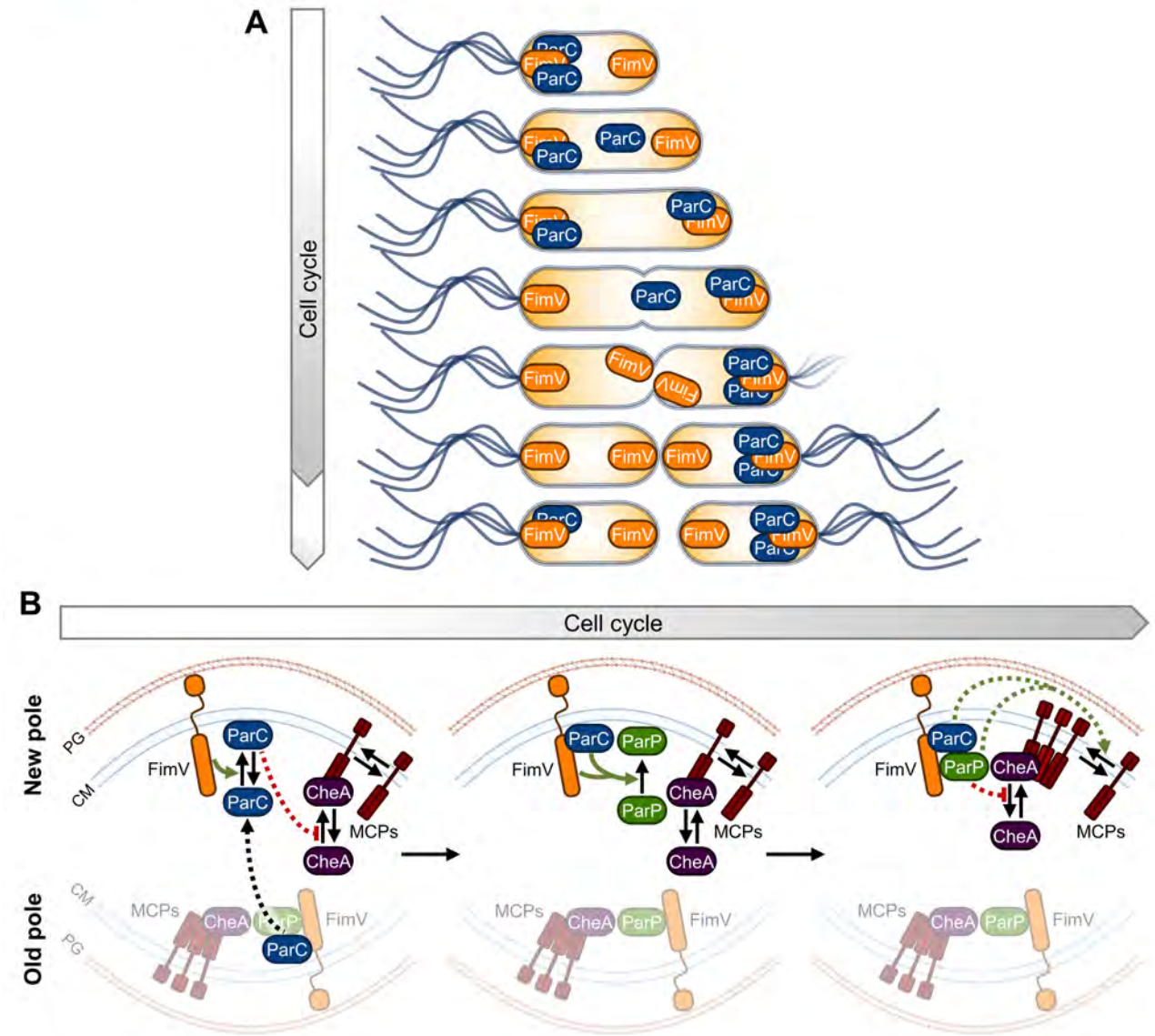

Figure 6. Working model of the polar localization of the chemotaxis arrays in *P. putida*. A. Cartoon depicting the FimV-dependent recruitment of ParC at the new cell pole during the cell cycle. **B.** Cartoon illustrating the hierarchical interactions between FimV, ParC and ParP that mediate localization of MCPs and CheA at the new cell pole during the cell cycle. Green arrows and T-shaped end red lines denote positive and negative effects, respectively. Dashed lines denote that interactions are indirect or have not been tested in this work. CM: cell membrane. PG: peptidoglycan.

REFERENCES

1. Altegoer F, Schuhmacher J, Pausch P, Bange G. 2014. From molecular evolution to biobricks and synthetic modules: a lesson by the bacterial flagellum. Biotechnol Genet Eng Rev 30:49-64.

2. Altschul SF, Gish W, Miller W, Myers EW, Lipman DJ. 1990. Basic local alignment search tool. J Mol Biol 215:403-410.

3. Alvarado A, Kjær A, Yang W, Mann P, Briegel A, Waldor MK, Ringgaard S. 2017. Coupling chemosensory array formation and localization. Elife 6:e31058.

4. Briegel A, Ladinsky MS, Oikonomou C, Jones CW, Harris MJ, Fowler DJ, Chang YW, Thompson LK, Armitage JP, Jensen GJ. 2014. Structure of bacterial cytoplasmic chemoreceptor arrays and implications for chemotactic signaling. Elife 3:e02151.

5. Canarini A, Kaiser C, Merchant A, Richter A, Wanek W. 2019. Root exudation of primary metabolites: mechanisms and their roles in plant responses to environmental stimuli. Front Plant Sci 10:157.

6. Choi KH, Gaynor JB, White KG, Lopez C, Bosio CM, Karkhoff-Schweizer RR, Schweizer HP. 2005. A Tn7-based broad-range bacterial cloning and expression system. Nat Methods 2:443-448.

7. Choi KH, Kumar A, Schweizer HP. 2006. A 10-min method for preparation of highly electrocompetent *Pseudomonas aeruginosa* cells: application for DNA fragment transfer between chromosomes and plasmid transformation. J Microbiol Methods 64:391-397.

8. Colin R, Ni B, Laganenka L, Sourjik V. 2021. Multiple functions of flagellar motility and chemotaxis in bacterial physiology. FEMS Microbiol Rev 45:fuab038.

9. de Lorenzo V, Pérez-Pantoja D, Nikel PI. 2024. *Pseudomonas putida* KT2440: the long journey of a soil-dweller to become a synthetic biology chassis. J Bacteriol 206(7):e0013624.

10. Dower WJ, Miller JF, Ragsdale CW. 1988. High efficiency transformation of *E. coli* by high voltage electroporation. Nucleic Acids Res 16:6127-6145.

11. Ducret A, Quardokus EM, Brun YV. 2016. MicrobeJ, a tool for high throughput bacterial cell detection and quantitative analysis. Nat Microbiol 1:16077.

12. Espinosa-Urgel M, Salido A, Ramos JL. 2000. Genetic analysis of functions involved in adhesion of *Pseudomonas putida* to seeds. J Bacteriol 182:2363-2369.

13. García-Fontana C, Reyes-Darias JA, Muñoz-Martínez F, Alfonso C, Morel B, Ramos JL, Krell T. 2013. High specificity in CheR methyltransferase function: CheR2 of *Pseudomonas putida* is essential for chemotaxis, whereas CheR1 is involved in biofilm formation. J Biol Chem 288:18987-18999.

14. Greenfield D, McEvoy AL, Shroff H, Crooks GE, Wingreen NS, Betzig E, Liphardt J. 2009. Self-organization of the *Escherichia coli* chemotaxis network imaged with super-resolution light microscopy. PLoS Biol 7:e1000137.

15. Grimm AC, Harwood CS. 1997. Chemotaxis of *Pseudomonas* spp. to the polyaromatic hydrocarbon naphthalene. Appl Environ Microbiol 63:4111-4115.

16. Hall BA, Armitage JP, Sansom MS. 2012. Mechanism of bacterial signal transduction revealed by molecular dynamics of Tsr dimers and trimers of dimers in lipid vesicles. PLoS Comput Biol 8:e1002685.

17. Harwood CS, Fosnaugh K, Dispensa M. 1989. Flagellation of *Pseudomonas putida* and analysis of its motile behavior. J Bacteriol 171:4063-4066.

18. Harwood CS, Parales RE, Dispensa M. 1990. Chemotaxis of *Pseudomonas putida* toward chlorinated benzoates. Appl Environ Microbiol 56:1501-1503.

19. Harwood CS, Rivelli M, Ornston LN. 1984. Aromatic acids are chemoattractants for *Pseudomonas putida*. J Bacteriol 160:622-628.

20. Hintsche M, Waljor V, Großmann R, Kühn MJ, Thormann KM, Peruani F, Beta C. 2017. A polar bundle of flagella can drive bacterial swimming by pushing, pulling, or coiling around the cell body. Sci Rep 7:16771.

21. Hu Z, Lutkenhaus J. 1999. Topological regulation of cell division in *Escherichia coli* involves rapid pole to pole oscillation of the division inhibitor MinC under the control of MinD and MinE. Mol Microbiol 34:82-90.

22. Inoue H, Nojima H, Okayama H. 1990. High efficiency transformation of *Escherichia coli* with plasmids. Gene 96:23-28.

23. Jones CW, Armitage JP. 2015. Positioning of bacterial chemoreceptors. Trends Microbiol 23:247-256.

24. Karimova G, Pidoux J, Ullmann A, Ladant D. 1998. A bacterial two-hybrid system based on a reconstituted signal transduction pathway. Proc Natl Acad Sci U S A 95:5752-5756.

25. Karimova G, Ullmann A, Ladant D. 2000. A bacterial two-hybrid system that exploits a cAMP signaling cascade in *Escherichia coli*. Methods Enzymol 328:59-73.

26. Lacal J, Muñoz-Martínez F, Reyes-Darías JA, Duque E, Matilla M, Segura A, Calvo JJ, Jímenez-Sánchez C, Krell T, Ramos JL. 2011. Bacterial chemotaxis towards aromatic hydrocarbons in Pseudomonas. Environ Microbiol 13:1733-1744.

27. Leal-Morales A, Pulido-Sánchez M, López-Sánchez A, Govantes F. 2022. Transcriptional organization and regulation of the *Pseudomonas putida* flagellar system. Environ Microbiol 24:137-157.

28. López-Farfán D, Reyes-Darias JA, Matilla MA, Krell T. 2019. Concentration dependent effect of plant root exudates on the chemosensory systems of *Pseudomonas putida* KT2440. Front Microbiol 10:78.

29. Luu RA, Schneider BJ, Ho CC, Nesteryuk V, Ngwesse SE, Liu X, Parales JV, Ditty JL, Parales RE. 2013. Taxis of *Pseudomonas putida* F1 toward phenylacetic acid is mediated by the energy taxis receptor Aer2. Appl Environ Microbiol 79:2416-2423.

30. Madeira F, Madhusoodanan N, Lee J, Eusebi A, Niewielska A, Tivey ARN, Lopez R, Butcher S. 2024.The EMBL-EBI Job Dispatcher sequence analysis tools framework in 2024. Nucleic Acids Res 52:521-525.

31. Mandelbaum RT, Wackett LP, Allan DL.1993. Mineralization of the s-triazine ring of atrazine by stable bacterial mixed cultures. Appl Environ Microbiol 59:1695-701.

32. Mauriello EMF, Jones C, Moine A, Armitage JP. 2018. Cellular targeting and segregation of bacterial chemosensory systems. FEMS Microbiol Rev 42:462-476.

33. Mileykovskaya E, Dowhan W. 2000. Visualization of phospholipid domains in *Escherichia coli* by using the cardiolipin-specific fluorescent dye 10-N-nonyl acridine orange. J Bacteriol 182:1172-1175.

34. Miller JH. 1993. A short course in bacterial genetics – A laboratory manual and handbook for *Escherichia coli* and related bacteria. Cold Spring Harbor, New York: Cold Spring Harbor Laboratory Press.

35. Miyata M, Robinson RC, Uyeda TQP, Fukumori Y, Fukushima SI, Haruta S, Homma M, Inaba K, Ito M, Kaito C, Kato K, Kenri T, Kinosita Y, Kojima S, Minamino T, Mori H, Nakamura S, Nakane D, Nakayama K, Nishiyama M, Shibata S, Shimabukuro K, Tamakoshi M, Taoka A, Tashiro Y, Tulum I, Wada H, Wakabayashi KI. 2020. Tree of motility - A proposed history of motility systems in the tree of life. Genes Cells 25:6-21.

36. Muok AR, Briegel A, Crane BR. 2020. Regulation of the chemotaxis histidine kinase CheA: a structural perspective. Biochim Biophys Acta Biomembr 1862:183030.

37. Navarrete B, Leal-Morales A, Serrano-Ron L, Sarrió M, Jiménez-Fernández A, Jiménez-Díaz L, López-Sánchez A, Govantes F. 2019. Transcriptional organization, regulation and functional analysis of *flhF* and *fleN* in *Pseudomonas putida*. PLoS One 14:e0214166.

38. Osterberg S, Skärfstad E, Shingler V. 2010. The sigma-factor FliA, ppGpp and DksA coordinate transcriptional control of the *aer2* gene of *Pseudomonas putida*. Environ Microbiol 12:1439-1451.

39. Parales RE, Ditty JL. 2018. Chemotaxis to atypical chemoattractants in soil bacteria. Methods Mol Biol 1729:255-280.

40. Parkinson JS. 1976. *cheA*, *cheB*, and *cheC* genes of *Escherichia coli* and their role in chemotaxis. J Bacteriol 126:758-770.

41. Pulianmackal LT, Vecchiarelli AG. Positioning of cellular components by the ParA/MinD family of ATPases. 2024. Curr Opin Microbiol 79:102485.

42. Pulido-Sánchez M, Leal-Morales A, López-Sánchez A, Cava F, Govantes F. 2025. Spatial, temporal and numerical regulation of polar flagella assembly in *Pseudomonas putida*. Microbiol Res 292:128033.

43. Raskin DM, de Boer PA. 1999. Rapid pole-to-pole oscillation of a protein required for directing division to the middle of *Escherichia coli*. Proc Natl Acad Sci U S A 96: 4971-4976.

44. Rico-Jiménez M, Roca A, Krell T, Matilla MA. 2022. A bacterial chemoreceptor that mediates chemotaxis to two different plant hormones. Environ Microbiol 24:3580-3597.

45. Ringgaard S, Schirner K, Davis BM, Waldor MK. 2011. A family of ParA-like ATPases promotes cell pole maturation by facilitating polar localization of chemotaxis proteins. Genes Dev 25:1544-1555.

46. Ringgaard S, Yang W, Alvarado A, Schirner K, Briegel A. 2018. Chemotaxis arrays in *Vibrio* species and their intracellular positioning by the ParC/ParP system. J Bacteriol 200:e00793-17.

47. Ringgaard S, Zepeda-Rivera M, Wu X, Schirner K, Davis BM, Waldor MK. 2014. ParP prevents dissociation of CheA from chemotactic signaling arrays and tethers them to a polar anchor. Proc Natl Acad Sci U S A 111:255-264.

48. Rodríguez-Herva JJ, Duque E, Molina-Henares MA, Navarro-Avilés G, Van Dillewijn P, De La Torre J, Molina-Henares AJ, La Campa AS, Ran FA, Segura A, Shingler V, Ramos JL. 2010. Physiological and transcriptomic characterization of a *fliA* mutant of *Pseudomonas putida* KT2440. Environ Microbiol Rep 2:373-380.

49. Rossmann F, Brenzinger S, Knauer C, Dörrich AK, Bubendorfer S, Ruppert U, Bange G, Thormann KM. 2015.The role of FlhF and HubP as polar landmark proteins in *Shewanella putrefaciens* CN-32. Mol Microbiol 98:727-742.

50. Rowlett VW, Margolin W. 2013. The bacterial Min system. Curr Biol 23:553-556.

51. Rudner DZ, Losick R. 2010. Protein subcellular localization in bacteria. Cold Spring Harb Perspect Biol 2:a000307.

52. Sambrook JE, Russell DW. 2000. Molecular cloning, a laboratory manual. Cold Spring Harbor, New York, USA: Cold Spring Harbor Laboratory Press.

53. Sarand I, Osterberg S, Holmqvist S, Holmfeldt P, Skärfstad E, Parales RE, Shingler V. 2008. Metabolism-dependent taxis towards (methyl)phenols is coupled through the most abundant of three polar localized Aer-like proteins of *Pseudomonas putida*. Environ Microbiol 10:1320-1334.

54. Schneider CA, Rasband WS, Eliceiri KW. 2012. NIH Image to ImageJ: 25 years of image analysis. Nat Methods 9:671-675.

55. Shiomi D, Yoshimoto M, Homma M, Kawagishi I. 2006. Helical distribution of the bacterial chemoreceptor via colocalization with the Sec protein translocation machinery. Mol Microbiol 60:894-906.

56. Sourjik V, Wingreen NS. Responding to chemical gradients: bacterial chemotaxis. 2012. Curr Opin Cell Biol 24:262-268.

57. Strahl H, Ronneau S, González BS, Klutsch D, Schaffner-Barbero C, Hamoen LW. 2015. Transmembrane protein sorting driven by membrane curvature. Nat Commun 6:8728.

58. Surovtsev IV, Jacobs-Wagner C. 2018. Subcellular organization: a critical feature of bacterial cell replication. Cell 172:1271-1293.

59. Thiem S, Kentner D, Sourjik V. 2007. Positioning of chemosensory clusters in *E. coli* and its relation to cell division. EMBO J 26:1615-1623.

60. Thiem S, Sourjik V. 2008. Stochastic assembly of chemoreceptor clusters in *Escherichia coli*. Mol Microbiol 68:1228-1236.

61. Thompson SR, Wadhams GH, Armitage JP. 2006. The positioning of cytoplasmic protein clusters in bacteria. Proc Natl Acad Sci U S A 103:8209-8214.

62. Valentini M, Laventie BJ, Moscoso J, Jenal U, Filloux A. 2016. The diguanylate cyclase HsbD intersects with the HptB regulatory cascade to control *Pseudomonas aeruginosa* biofilm and motility. PLoS Genet 12:e1006354.

63. Wadhams GH, Armitage JP. 2004. Making sense of it all: bacterial chemotaxis. Nat Rev Mol Cell Biol 5:1024-1037.

64. Yamaichi Y, Bruckner R, Ringgaard S, Möll A, Cameron DE, Briegel A, Jensen GJ, Davis BM, Waldor MK. 2012. A multidomain hub anchors the chromosome segregation and chemotactic machinery to the bacterial pole. Genes Dev 26:2348-60.

1 **65.** Yang W, Briegel A. 2020. Diversity of bacterial chemosensory arrays. Trends Microbiol
2 28:68-80.